Effects of shell thickness on the thermal stability of Cu-Ag core-shell nanoparticles A molecular dynamics study

Li, Shizhen; Liu, X.; Jiang, Jing; Tan, Chunjian; Gao, Chenshan; Liu, Yang; Ye, H.; Zhang, Guoqi

DOI
10.1109/EuroSimE54907.2022.9758874

Publication date
2022

Document Version
Final published version

Published in
Proceedings of the 2022 23rd International Conference on Thermal, Mechanical and Multi-Physics Simulation and Experiments in Microelectronics and Microsystems (EuroSimE)

2022 23rd International Conference on Thermal, Mechanical and Multi-Physics Simulation and Experiments in Microelectronics and Microsystems (EuroSimE) | 978-1-6654-5836-8/22/$31.00 ©2022 IEEE | DOI: 10.1109/EuroSimE54907.2022.9758874

Effects of shell thickness on the thermal stability of Cu-Ag core-shell nanoparticles: a molecular dynamics study

Shizhen Li [a], Xu Liu [a,b], Jing Jiang[c], Chunjian Tan [a,b], Chenshan Gao [a,d], Yang Liu [e], Huaiyu Ye [a,d*], Guoqi Zhang [b *]
a School of Microelectronics, Southern University of Science and Technology, Shenzhen 518055, China
b Department of Microelectronics, Delft University of Technology, 2628 CD Delft, the Netherlands
c Academy for Engineering&Technology, Fudan University, Shanghai 200433, China.
d The Key Laboratory of Optoelectronic Technology &Systems, College of Optoelectronic Engineering, Education Ministry of China, Chongqing University, Chongqing 400044, China
e School of Materials Science and Chemical Engineering, Harbin University of Science and Technology, Harbin, 150040, China
* Corresponding authors: h.ye@tudelft.nl

Abstract

Cu-Ag core-shell (CS) nanoparticle (NP) is considered as a cost-effective alternative material to nano silver sintering material in die attachment application. To further reduce the cost, the thickness of the Ag shell can be adjusted. Whereas the shell thickness will also affect the thermal stability of the Cu-Ag CSNPs. In this study, molecular dynamics simulation was applied to study the thickness effect on the thermal behavior of Cu-Ag CSNPs. The melting points of CSNPs and Pure NPs can be determined by the evolutions of Potential Energy (PE), and the Lindemann index (LI) of the system. The results indicated that the melting points of CS NPs were lower than monometallic NP and the melting point of CS NP is influenced by the size of the Cu core and the number of lattice mismatches. Moreover, the distribution of atoms' LI showed that the premelting point is independent of shell thickness. However, the fraction of atoms that occurred premelting is increased with the decrease of the shell thickness. Otherwise, we also simulated the sintering process of double CS NPs with equal size.

1. Introduction

With the developments of high-power electronic devices, there is a great demand for the die-attach solution for high-temperature service[1,2]. Compared with their bulk counterparts, NPs have larger surface curvature, higher surface energy, better conductivity, and lower melting temperatures[3]. Sintered Ag NPs have been used as an interconnection structure in power electronics due to its good thermal, electrical, and mechanical properties[4–6]. However, Ag limits its extensive applications in the industry because of its high cost[7]. Cu is proposed as a substitution of Ag due to its low cost as well as good thermal and electrical property[8]. But pure Cu in nanosize performs very poor anti-oxidation property[9]. Cu-Ag core-shell nanoparticles (CS NPs) are synthesized as a substitute for Ag NPs[10]. Cu-Ag core-shell structure provides not only protection for the oxidation of copper nanoparticles but also a reduction of the ion migration of silver nanoparticles. Moreover, the cost of Cu-Ag CS NPs is much lower than the Ag NPs[11].

The sintering is one of the most important metallurgic methods for nanojoining and inkjet printing technology[12]. The thermal stability directly effects the sintering property which is related to the sintered structure. Therefore, it is necessary to investigate and understand the thermal stability and melting behaviors of Cu-Ag CS NPs. Since the effects of size on thermal stability had been studied by other researchers, we will simulate the Cu-Ag CS NPs with different shell thicknesses by molecular dynamics simulation. At the end of the study, we also simulated the sintering process of double CS NP

2. Method and computational details

The embedded atom method (EAM) has been widely adopted in metallic nanoparticle interaction study. Thus, in our simulation, we selected the Cu-Ag embedded atom method (EAM) potential of the alloy system[13]. The crystalline model parameters, like lattice parameter, elastic constants, and thermal expansion, can be precisely reproduced by this binary EAM potential[14]. According to this potential model, the total energy existed in the Cu-Ag system is expressed as:

$$E_{tot} = \frac{1}{2}\sum_{ij} V_{ij}(r_{ij}) + \sum_i F_i(\overline{\rho_i}). \quad (1)$$

Here is the pair interaction energy of atoms i and j with a distance of , the embedding energy of atom I as a function of the host electron density . The is given by

$$\overline{\rho_i} = \sum_{j\neq i} \rho_j(r_{ij}), \quad (2)$$

in which is the electron density function of atom i assigned to atom j.

Each CS NP has been relaxed separately at corresponding sintering temperature for 500 ps to reach a stable CS structure in sintering simulation. And for melting simulation, each CS NP was relaxed at 300K. Both melting and sintering processes were used the equilibrated NPs as initial structures. We applied the isothermal-heating method (IH) to eliminate the thermal gradient. Therefore, the effect of heat transfer during melting and sintering can be eliminated.

The simulations were conducted with LAMMPS code[15]. NVT canonical ensemble, and the Nosé-Hoover thermostat control were used to control the temperature. We set 1 fs and 100 ps as the time step and the simulation duration respectively.

PE and Lindemann index (LI, δ_{LI}) were normally used to calculate the melting points (MPs) of nano material[16]. In the melting process, after the absorption of latent, the PE curve reaches the reflection point which can determine the melting point. The LI is a simple measure of thermally driven disorder in atoms or molecules, which can determine the temperature in the melting transition phase of the nanoparticles and the MPs at which LI curves

978-1-6654-5836-8/22/$31.00 ©2022 IEEE

increases rapidly. The local Lindemann index is defined as[17]:

$$\delta_{LI,i} = \frac{1}{N-1}\sum_{j\neq i}\frac{\sqrt{\langle r_{ij}^2\rangle - \langle r_{ij}\rangle^2}}{\langle r_{ij}\rangle} \quad (3)$$

where N is the total number of atoms in the system, r_{ij} the distance between i-th and j-th atoms,

and $\langle\ \rangle$ the ensemble average. The LI of the system can be defined as:

$$\delta_{LI} = \frac{1}{N}\sum_i \delta_{LI,i} \quad (4)$$

which is the average of all atoms' LI. For LI value, 0.7 and 0.1, respectively, are the melting criteria of pure Ag and pure Cu atoms. If the LI value of an atom is higher than the criteria, then that atom is defined as Lindemann atom.

The shrinkage is defined as the change in the center-to-center distance of the particles over the initial distance, given by[18]:

$$\zeta = \frac{\Delta L}{L_0} = \frac{L_0 - L}{L_0} \quad (5)$$

Where L_0 is the initial distance between the centers of two NPs at the beginning of sintering, and L is the instantaneous distance of centers varied with sintering time.

3. Results and discussion

Melting simulation

The specific data and models of each NP were shown in Table 1. NP 1 and NP5 are monometallic NPs consisted of Ag and Cu respectively. NP2, NP3, NP4 were Cu-Ag CS NPs with various thicknesses of Ag shell. And the Ag atoms layers outside the Cu core are 5 layers, 3 layers, and 1 layer, respectively. All five types of NPs are built with the same total number of atoms. The thermal stabilities of five types of Cu-Ag CS NPs were studied. These simulations could identify melting points and melting processes. The surface premelting of NPs could facilitate shrinkage growth 错误!未找到引用源。. Among the melting simulations, we employed the isothermal heating method to eliminate the thermal gradient inside the NPs. The simulation was performed at a series of temperatures between 300K and 1400K. 100K and 20K, respectively, are selected as the temperature interval of 300K to 700K and 700K to 1400K.

The melting point can be deduced from the temperature-dependent potential energy profile and LI profile from Figs. 1(a) and (b). The melting points were determined as 1103K, 997K, 956K, 1080K, and 1160K for NP1, NP2, NP3, NP4 and NP5 respectively. All of the core-shell NPs had lower melting points than monometallic NPs.

Table 1. Configuration of Cu-Ag core-shell NPs with five different types

NP items / Atom Numbers	NP1	NP2	NP3
			
Total	2123	2123	2123
Ag	2123	1874	1440
Cu	0	249	683
NP items / Atom Numbers	**NP4**	**NP5**	
			
Total	2123	2123	
Ag	618	0	
Cu	1505	2123	

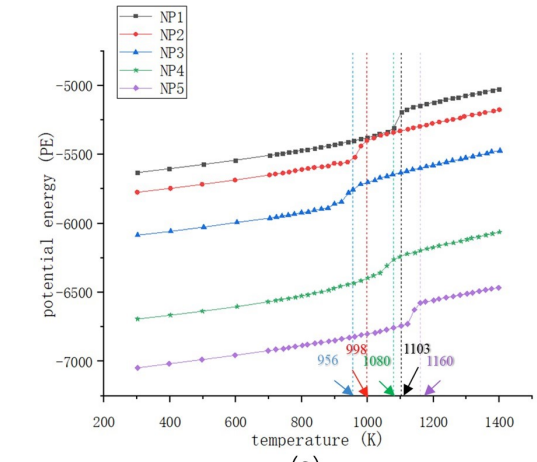

(a)

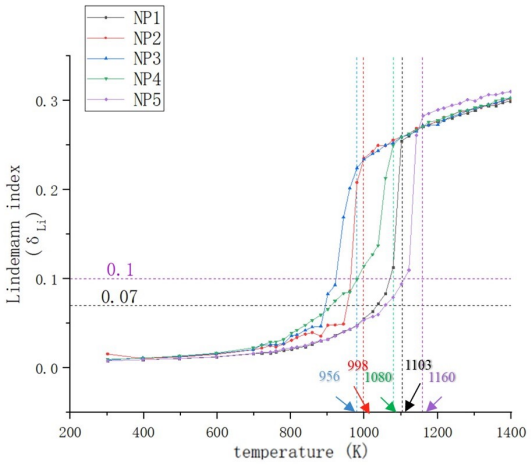

(b)

Figure 1. Potential energy (PE) and lindemann index (δ_{LI}) of systems for all types of NPs during IH process.

The Lindemann indexs (δ_{LI}) of each atom was shown in Fig. 2. The atoms on the surface of the particles and the Ag and Cu at the interface of CS NPs

showed higher activity. In the initial state (300K), the outermost of NP4 showed higher mobility than other NPs. The LI of Ag atoms located at the surface had a certain rising as the temperature increase, especially for NP3 and NP4. When the temperature continued to rise to 700K, some Ag atoms of CS NPs on the surface had become Lindemann atoms determined by δ_{LI} above δ_c, which means surface premelting occurs. We can find that the shell thickness had no obvious effect on the premelting temperature but can affect the state of surface premelting. With the temperature increasing, surface premelting transferred from the outer part to the inner part, previous research had reported this phenomenon[19]. At 880K, the silver shell of NP4 was almost melting, while other CS NPs still had a part of LI of atoms of shell lower than δ_c. When the temperature reached 940K, NP3 had completed the process of solid–liquid phase transition, both Ag shell and Cu core were liquid phases, and the Cu atoms neared interface diffused from the core to shell. Although the melting point of NP4 was much higher than other CS NPs, its outermost atoms had higher mobility.

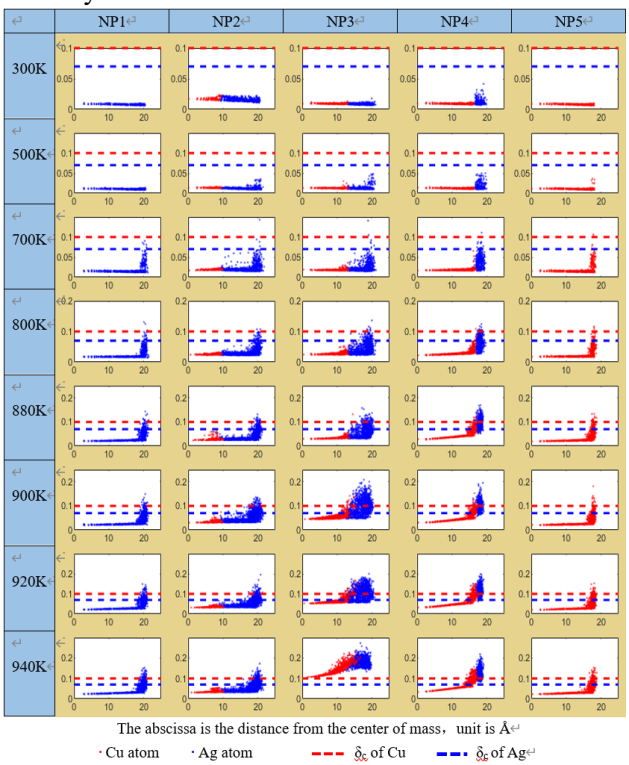

Figure 2. Lindemann index (LI, δ_{LI}) of each atom along the radius of 5 types of NP at representative temperatures. Red plot and blue plot represent LI of Cu and Ag respectively. The red dotted line is the δ_c of Cu, and the blue dotted line is the δ_c of Ag.

Sintering simulation

To investigate the effects of varying shell thickness on the sintering process of CS NPs, five types of NPs with the same structures of melting simulation were selected to conduct the sintering simulations at various temperatures. To ensure the sintering process start at an equilibrium state, the initial structure was relaxed at 300K before sintering simulations.

Table 2 is the final shrinkages of five types of NP sintering at four temperatures. Compared to monometallic NPs, CS NPs had higher shrinkage at the same sintering temperature and were more sensitive to temperature because of the existence of the amorphous

Table 2 the result of shrinkages sintering at 500K, 700K, 900K, 950K for five types of NPs pair

	NP1	NP2	NP3	NP4	NP5
500K	0.0831	0.0985	0.1048	0.1196	0.0942
700K	0.0898	0.1558	0.1661	0.1710	0.1391
900K	0.0941	0.2353	0.2874	0.3526	0.1401
950K	0.1288	0.4281	0.8042	0.4235	0.1895

atoms located at the interface of Cu and Ag. The shrinkage of CS NPs with varying shell thickness also had some differences. At 500K, the shrinkage of NP4 was 14.12% larger than that of NP3 and 21.42% larger than that of NP2.

At 700K, the shrinkage of NP4 was only 2.9% larger than that of NP3 and 9.7% larger than that of NP2. The effect of shell thickness on shrinkage experienced a significant decrease. But when the temperature rose to 900K, the shrinkage of NP4 is 22.7% larger than that of NP3 and 44.9% larger than that of NP2, the effect of shell thickness became even more significant than 500K. The shrinkage increases with decreasing shell thickness. The significance of shell thickness to shrinkage is also partly dependent upon sintering temperature.

At 950K, it was observed that the shrinkage of NP3 was much larger than NP4, and NP2 has a similar shrinkage to NP4. The temperature was almost reaching the melting temperature of NP3, and the liquid phase dominated in sintering structure which made the sintering process was mainly performed in the liquid phase. Therefore, the shell thickness was no longer an important influence factor of shrinkage in the liquid phase sintering.

The sintering process can be characterized by three stages as illustrated in shrinkage curves (Figs. 3(a)-(c)). Stage II was sensitive to temperature and shell thickness. The CS NPs with varying shell thicknesses appeared different sintering process in stage II. In most cases, the increase of shrinkage at low temperatures in stage II is not very obvious. At 500K, compared with other NPs, the shrinkage of NP4 had an increase from 10 ps to 50 ps.

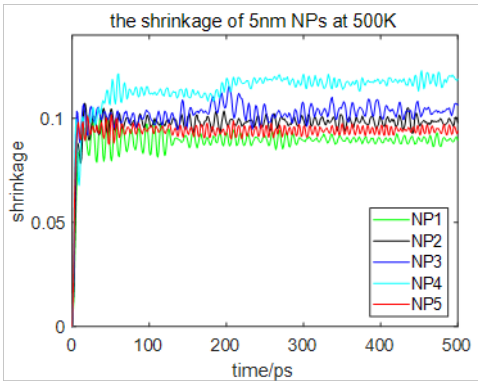

(a)

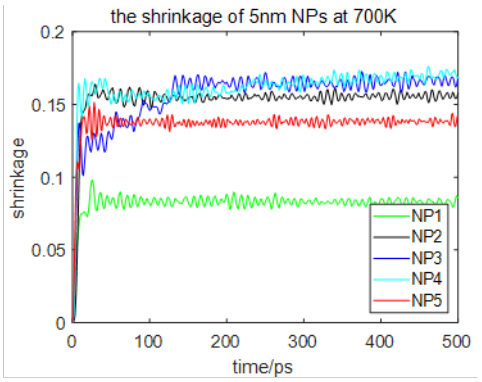

(b)

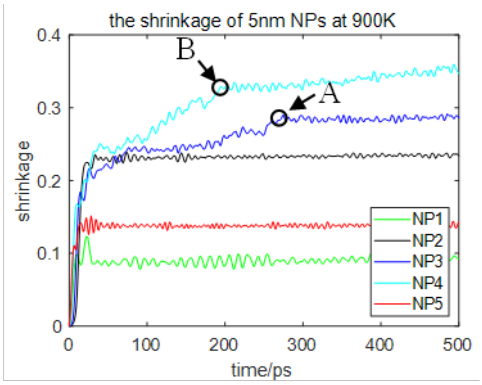

(c)

Figure 3. (a) the shrinkage of NPs at 500K (b) the shrinkage of NPs at 700K (c) the shrinkage of NPs at 900K

4. Conclusions

Melting simulations were conducted to identify the melting points of NPs. Core-shell nanoparticles have lower melting points than monometallic nanoparticles. With the decreasing of shell thickness, the LI (Lindermann Index) of outermost atoms of both shell layer and core layer became higher, which means the mobility of outermost atoms increases with decreasing the shell thickness. The shrinkage was used to characterize the sintering process. The final shrinkage increased as the Ag shell thickness got thinner. The grain boundary diffusion can be found in NP4 at 500K, 700K, and 900K, as well as NP3 at 900K after the formation of the neck.

Acknowledgments

This work was supported by the National Key R&D Program of China (2018YFE0204600), the Shenzhen Fundamental Research Program (JCYJ20200109140822796), and the NSQKJJ under grant K21799119.

References

[1] J.G. Bai, J. Yin, Z. Zhang, G.-Q. Lu, J.D. van Wyk, High-Temperature Operation of SiC Power Devices by Low-Temperature Sintered Silver Die-Attachment, IEEE TRANSACTIONS ON ADVANCED PACKAGING. 30 (2007) 5.

[2] H. Ji, J. Zhou, M. Liang, H. Lu, M. Li, Ultra-low temperature sintering of Cu@Ag core-shell nanoparticle paste by ultrasonic in air for high-temperature power device packaging, Ultrasonics Sonochemistry. 41 (2018) 375–381. https://doi.org/10.1016/j.ultsonch.2017.10.003.

[3] P. Buffat, J.-P. Borel, Size effect on the melting temperature of gold particles, Phys. Rev. A. 13 (1976) 2287–2298. https://doi.org/10.1103/PhysRevA.13.2287.

[4] Y. Zhong, R. An, C. Wang, Z. Zheng, Z.-Q. Liu, C.-H. Liu, C.-F. Li, T.K. Kim, S. Jin, Low Temperature Sintering Cu6Sn5 Nanoparticles for Superplastic and Super-uniform High Temperature Circuit Interconnections, Small. (2015) 7.

[5] H.A. Alarifi, M. Atis, C. Özdoğan, A. Hu, M. Yavuz, Y. Zhou, Molecular dynamics simulation of sintering and surface premelting of silver nanoparticles, Materials Transactions. 54 (2013) 884–889. https://doi.org/10.2320/matertrans.MD201225.

[6] C. Chen, K. Suganuma, Microstructure and mechanical properties of sintered Ag particles with flake and spherical shape from nano to micro size, Materials & Design. 162 (2019) 311–321. https://doi.org/10.1016/j.matdes.2018.11.062.

[7] H.T. Hai, H. Takamura, J. Koike, Oxidation behavior of Cu-Ag core-shell particles for solar cell applications, Journal of Alloys and Compounds. 564 (2013) 71–77. https://doi.org/10.1016/j.jallcom.2013.02.048.

[8] C. Yang, C.P. Wong, M.M.F. Yuen, Printed electrically conductive composites: Conductive filler designs and surface engineering, Journal of Materials Chemistry C. 1 (2013) 4052–4069. https://doi.org/10.1039/c3tc00572k.

[9] Z. Jiang, Y. Tian, S. Ding, Synthesis and characterization of ultra-long and pencil-like copper nanowires with a penta-twinned structure by hydrothermal method, Materials Letters. 136 (2014)

310–313. https://doi.org/10.1016/j.matlet.2014.08.033.
[10] C. Lee, N.R. Kim, J. Koo, Y.J. Lee, H.M. Lee, Cu-Ag core–shell nanoparticles with enhanced oxidation stability for printed electronics, Nanotechnology. 26 (2015) 455601. https://doi.org/10.1088/0957-4484/26/45/455601.
[11] B. Cheng, A.H.W. Ngan, The crystal structures of sintered copper nanoparticles: A molecular dynamics study, International Journal of Plasticity. 47 (2013) 65–79. https://doi.org/10.1016/j.ijplas.2013.01.006.
[12] J.S. Raut, R.B. Bhagat, K.A. Fichthorn, Sintering of aluminum nanoparticles: A molecular dynamics study, Nanostructured Materials. 10 (1998) 837–851. https://doi.org/10.1016/S0965-9773(98)00120-2.
[13] M.S. Daw, M.I. Baskes, Embedded-atom method: Derivation and application to impurities, surfaces, and other defects in metals, Physical Review B. 29 (1984) 6443–6453. https://doi.org/10.1103/PhysRevB.29.6443.
[14] P.L. Williams, Y. Mishin, J.C. Hamilton, An embedded-atom potential for the Cu-Ag system, Modelling and Simulation in Materials Science and Engineering. 14 (2006) 817–833. https://doi.org/10.1088/0965-0393/14/5/002.
[15] S. Plimpton, Fast Parallel Algorithms for Short-Range Molecular Dynamics, Modelling and Simulation in Materials Science and Engineering. 18 (2009) 44. https://doi.org/10.1006/jcph.1995.1039.
[16] Y. Tamura, N. Arai, Molecular dynamics simulation of the melting processes of core–shell and pure nanoparticles, Molecular Simulation. 41 (2015) 905–912. https://doi.org/10.1080/08927022.2014.976636.
[17] Y. Shibuta, T. Suzuki, Melting and nucleation of iron nanoparticles: A molecular dynamics study, Chemical Physics Letters. 445 (2007) 265–270. https://doi.org/10.1016/j.cplett.2007.07.098.
[18] P. Song, D. Wen, Molecular dynamics simulation of the sintering of metallic nanoparticles, Journal of Nanoparticle Research. 12 (2010) 823–829. https://doi.org/10.1007/s11051-009-9718-7.
[19] G.J. Ackland, A.P. Jones, Applications of local crystal structure measures in experiment and simulation, Physical Review B - Condensed Matter and Materials Physics. 73 (2006) 1–7. https://doi.org/10.1103/PhysRevB.73.054104.